International Journal of Multiphase Flow 35 (2009) 885–895

Contents lists available at ScienceDirect

International Journal of Multiphase Flow

journal homepage: www.elsevier.com/locate/ijmulflow

# Numerical and experimental study on effect of wall geometry on wall impingement process of hollow-cone fuel spray under various ambient conditions

Young-Sam Shim [a], Gyung-Min Choi [b,*], Duck-Jool Kim [b]

[a] School of Mechanical Engineering, Pusan National University, Busan 609-735, Republic of Korea
[b] Pusan Clean Coal Center, School of Mechanical Engineering, Pusan National University, Busan 609-735, Republic of Korea

ARTICLE INFO

*Article history:*
Received 13 November 2008
Received in revised form 21 April 2009
Accepted 16 June 2009
Available online 27 June 2009

*Keywords:*
GDI (gasoline direct injection)
Fuel film
Hollow-cone fuel spray
Spray vaporization
Spray–wall impingement

ABSTRACT

The spray–wall impingement process in gasoline direct injection (GDI) engines, which is caused by the interaction among spray, wall and air to move the air–fuel mixture near the spark plug, directly influences the engine performance and emissions. Therefore, a detailed understanding of this process is very important in designing an injection system and controlling a strategy of GDI engines. The purpose of this study is to understand the spray–wall impingement characteristics for more efficient designing of the injection system in GDI engines and to supply the fundamental data under engine operation conditions. The wall impingement processes of hollow-cone fuel spray according to ambient gas conditions and wall geometry are calculated by validated spray models. The calculated results were compared with the experimental results obtained by the laser-induced exciplex fluorescence (LIEF) technique. It was found that the spray and vortex cloud at the high ambient pressure were distributed at inner area of cavity and the more fuel film mass observed at this condition. The fuel film mass decreased with the increase of ambient temperature, while the fuel film mass increased at high cavity angles.



## 1. Introduction

Gasoline direct injection (GDI) engines have the potential to remarkably reduce the fuel consumption and increase the engine performance (Zhao et al., 1999). GDI engines, however, have emission problems such as excessive light-load unburned hydrocarbons and even particulate emissions at late fuel injection. These emission problems are strongly affected by fuel stratification and spray–wall interaction, which is unavoidable in GDI engines (Drake et al., 2003). Also, the wall impingement of liquid fuel spray on the combustion chamber wall is generally one of the major drawbacks of GDI engines because it increases HC emissions and have great effect on the combustion process. However, in wall-guided stratified-charged combustion mode at late injection, the impingement of GDI spray on the wall is intended to distribute the rich mixture near spark plug for successful ignition and stable combustion. Therefore it is important to obtain a detailed understanding of the spray–wall impingement process and its effects on the spray characteristics and to provide fundamental data for validation of CFD predictions, which have become indispensable in the design of GDI engines.

Numerous researches on the spray–wall impingement have been performed by the experimental and numerical methods. Park et al. (1999) characterized the GDI spray–wall interaction inside a heated pressurized chamber using various visualization techniques. They found that upward spray vortex inside the spray is more obvious at the high temperature condition and more rapid impingement and faster horizontal spread after impingement are observed for the high temperature condition. Lindgren and Denbratt (2000) investigated the prediction capability of spray–wall impingement models, such as the Watkins model (Walkins and Park, 1996), the Gosman model (Bai and Gosman, 1995) and the Fujimoto model (Senda et al., 1994). They found that models based on single-droplet experiments are insufficient to calculate the spray–wall impingement process. Also, calculated results of tangential velocity after the spray–wall impingement were smaller than experimental results. In spite of the previous efforts, further researches on the effect of the ambient conditions and wall geometry on the spray–wall impingement are still required because the previous researches focused mainly on the diesel spray impingements. Therefore, the wall impingement of hollow-cone fuel spray in GDI engines must be studied because spray structure and injection pressure are different from those of diesel engines.

In this study, the numerical analyses of the wall impingement process, vaporization process and air–fuel mixture formation of hollow-cone fuel spray according to the ambient gas characteristic and wall geometry are presented for the detail understanding of

* Corresponding author. Address: School of Mechanical Engineering, Pusan National University, 30 Jangjeon-dong, Geumjeong-gu, Busan 609-735, Republic of Korea. Tel.: +82 (0) 51 510 2476; fax: +82 (0) 51 512 5236.
*E-mail address:* choigm@pusan.ac.kr (G.-M. Choi).

0301-9322/$ - see front matter © 2009 Elsevier Ltd. All rights reserved.
doi:10.1016/j.ijmultiphaseflow.2009.06.004

the spray–wall impingement affecting the performance and emissions of GDI engines. The ambient pressures were 0.1 and 0.5 MPa and the ambient temperatures were 293 and 473 K. The cavity angles of 0°, 30°, 60° and 90° were adopted to understand the effect of the wall geometry on the spray structure in detail. The LISA (linearized instability sheet atomization)–APTAB (aerodynamically progressed Taylor analogy breakup) model (Shim et al., 2008), the high-pressure vaporization model (Abramzon and Sirignano, 1989) and the Gosman model (Bai and Gosman, 1995) were adopted to calculate the atomization, vaporization and wall impingement processes, respectively.

## 2. Spray models

In this study, the LISA–APTAB model, the modified Abramzon model and the Gosman model were used for the atomization, vaporization and wall impingement processes, respectively. An aerodynamic drag was calculated with drag and distortion model (Liu et al., 1993). The occurrence of collision and coalescence was calculated with the O'Rourke model (O'Rourke, 1981). A RNG $k$–$\varepsilon$ model was used for a turbulence calculation (Han and Reitz, 1995). To calculate the fuel film vaporization, the model used in the KIVA code was adopted (Amsden, 1997).

### 2.1. Hybrid breakup model (Shim et al., 2008)

This model is divided into three stages, that is, film formation, sheet breakup and atomization as shown in Fig. 1. The film formation and sheet breakup are called primary breakup process and the atomization is called secondary breakup process. The sheet breakup process includes the effects of the surrounding gas, liquid viscosity and surface tension on the breakup of the liquid sheet. The sheet will breakup and ligaments will be formed at a length given by

$$L = U\tau = \frac{U}{\Omega}\ln\left(\frac{\eta_b}{\eta_0}\right) \tag{1}$$

where the quantity $\ln(\eta_b/\eta_0)$ is 12. This value is based on the study conducted by Dombrowski and Hooper (1962). If it is assumed that breakup occurs when the amplitude of the unstable waves is equal to the radius of ligament, one droplet will be formed per wavelength. A mass balance then gives

$$d_D^3 = \frac{3\pi d_L^2}{K_L} \tag{2}$$

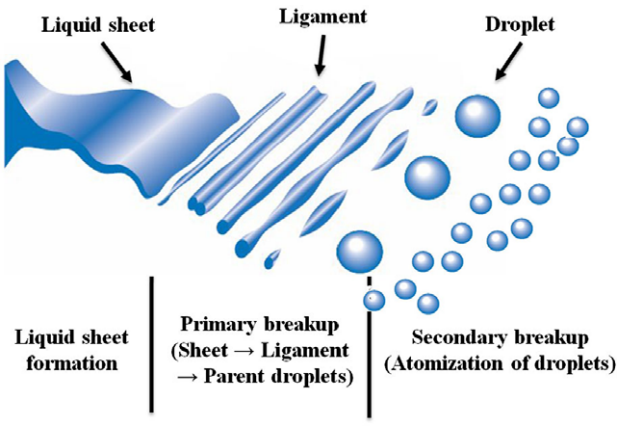


**Fig. 1.** Breakup mechanism of liquid sheet in hollow-cone fuel spray.

where $K_L$ is the most unstable wavelength on the ligament. In the previous stage of the model, the droplets are introduced into the domain and initialized.

The APTAB model was used for the secondary breakup model. In this model, it is discovered that the deformed droplet shape is an oblate spheroid having an ellipsoidal cross-section. The model equation is given by

$$\ddot{y} + \frac{5N}{\mathrm{Re}K}\dot{y} + \frac{1}{K}\left[\frac{8}{We} - \frac{8}{19} - \frac{2}{19}y\right]y = \frac{8}{19K} \tag{3}$$

where the value of $K$ is $\rho_l/\rho_g$ and the value of $N$ is $\mu_l/\mu_g$. The solution of this equation is gotten by the fourth order Runge–Kutta method. The breakup criteria are given by

$$2(1+0.5y)^5 + (1+0.5y)^{-1} - 4(1+0.5y)^{-4} > C_b We \tag{4}$$

### 2.2. Spray vaporization model

The high-pressure vaporization model (Abramzon and Sirignano, 1989) considering the 'film theory' was used for spray vaporization process. The film theory assumes that the resistance to heat or mass exchange between surface and the surrounding gas flow can be modeled by introducing the concept of gas films of constant thicknesses. The total mass rate flow through this surface will be equal to the vaporization rate

$$\dot{m}_F = 2\pi r_s \rho_g D_g Sh^* \ln(1+B_M) \tag{5}$$

$$\dot{m}_F = 2\pi r_s \frac{k_g}{C_{pg}} Nu^* \ln(1+B_T) \tag{6}$$

where subscripts $s$ and $g$ refer to the droplet surface and gas, respectively. The value $B_M$ and $B_T$ are the Spalding mass and heat transfer numbers, and they are calculated as

$$B_M = \frac{Y_{F_s} - Y_{F_\infty}}{1 - Y_{F_s}} \tag{7}$$

$$B_T = \frac{c_{pg}(T_\infty - T_s)}{L(T_s) + Q_L/\dot{m}_F} \tag{8}$$

where $Y_F$ is fuel mass fraction and $L(T_s)$ is the latent heat of vaporization at temperature $T_s$. $Q_L$ is the heat penetrating into the droplet and can be expressed by

$$Q_L = \dot{m}_F\left\{\frac{c_{pg}(T_\infty - T_s)}{B_T} - L(T_s)\right\} \tag{9}$$

Eqs. (7) and (8) are similar to the expressions for the droplet vaporization rate predicted by the classical model, with the values of the non-dimensional parameters $Sh_0$ and $Nu_0$ in the classical formulas substituted by $Sh^*$ and $Nu^*$, respectively. These are expressed as

$$Sh^* = 2 + \frac{(Sh_0 - 2)}{F(B_M)} \tag{10}$$

$$Nu^* = 2 + \frac{(Nu_0 - 2)}{F(B_T)} \tag{11}$$

where the parameters $Sh^*$ and $Nu^*$ are the modified Nusselt and Sherwood numbers, and tend to $Sh_0$ and $Nu_0$, respectively, as $F(B_M)$ and $F(B_T)$ tend to the unity and $F(B)$ is the universal function

$$F(B) = (1+B)^{0.7}\frac{\ln(1+B)}{B} \tag{12}$$

The $Sh_0$ and $Nu_0$ are evaluated by the Frossling correlations and expressed as

$$Sh_0 = 2 + 0.6\sqrt{\mathrm{Re}}Sc^{1/3} \tag{13}$$

$$Nu_0 = 2 + 0.6\sqrt{\mathrm{Re}}\mathrm{Pr}^{1/3} \tag{14}$$

The accuracy of the above equation is dependent on how the thermo-physical properties are evaluated. It has been recommended to use the one-third rule and the mixture rule where the properties, such as $c_p$, $k$ and $\mu$, are evaluated at a reference temperature and composition.

### 2.3. Wall impingement model

The spray–wall impingement model developed by Bai and Gosman (1995) is based on various experimental results and considers both the dry and the wet walls. They divided the impingement phenomenon into 10 regimes by the different conditions of impinging droplets. Fig. 2 shows a qualitative map of the impingement regimes and the associated transition regimes in a two-dimensional space with the Weber numbers and the wall temperatures as coordinates.

### 2.4. Calculation condition

The calculations were performed in a calculation domain of 80 mm × 80 mm and the grid size was 1 mm × 1 mm. The number of discrete droplet parcels was 5000 and these droplet parcels were injected into a quiescent air environment with an injection period of 2.0 ms. Other conditions are indicated in Table 1.

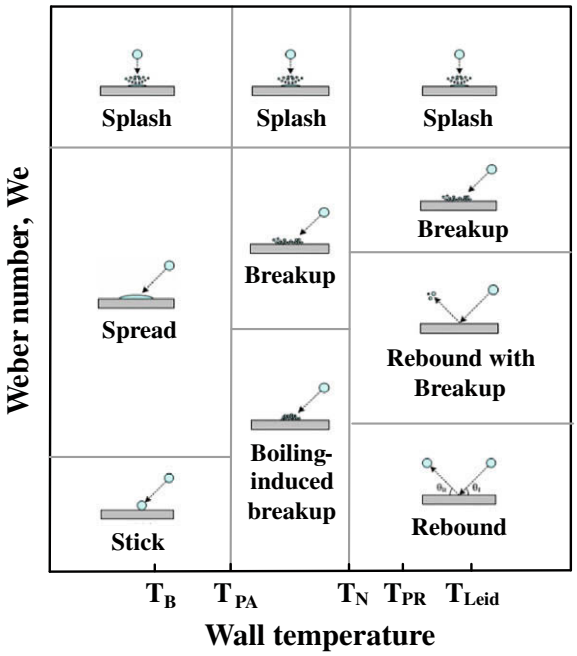


**Fig. 2.** Schematic of different impaction regimes and overview of droplet impingement regimes and transition conditions for a dry wall (Bai and Gosman, 1995).

**Table 1**
Experiment and calculation conditions.

| Fuel | Hexane/fluorobenzene/DEMA |
|---|---|
| Injection pressure (MPa) | 5.1 |
| Injection duration (ms) | 2.0 |
| Injection quantity (mg) | 15 |
| Ambient gas | $N_2$ |
| Ambient temperature (K) | 293, 473 |
| Ambient pressure (MPa) | 0.1, 0.5 |
| Impingement distance (mm) | 46.7 |
| Cavity diameter (mm) | 30 |
| Cavity angle (°) | 0, 30, 60, 90 |

## 3. Experimental setup and method

### 3.1. Experimental setup

Fig. 3 shows a schematic diagram of the experimental setup of the LIEF technique used for investigating the spray characteristics of the GDI injector. The spray chamber was designed to measure the behavior and structure of the hollow-cone fuel spray under various ambient conditions. The possible maximum ambient temperature and pressure are 600 K and 3 MPa, respectively. Nitrogen was purged as the ambient gas to prevent the quenching of liquid fluorescence by oxygen. The fourth harmonic of the Nd:YAG at 266 nm with duration of 7 ns and a laser energy of 50 mJ/pulse was used to excite dopants from the fuel sprays. The laser beam formed a thin light sheet of 60 mm high and less than 400 μm thick. The filters were 400 ± 25 nm for liquid phase. An additional WG280 sharp cut filter was used to eliminate the light at 266 nm. The spray images were digitally recorded with an intensified CCD camera that provided 640 by 480 pixel images at a resolution of 8 bits and was mounted perpendicular to the laser sheet. The camera system consisted of a personal computer with an image grabber, a shutter controller and a pulse generator. In order to inject the fuel with high pressure and to avoid pressure fluctuations in the fuel rail, a compressed nitrogen cylinder and hydraulic accumulator were used. A high pressure swirl injector with 70° was used.

### 3.2. Experimental method

In the LIEF technique, the exciplex system of fluorobenzene and DEMA in a non-fluorescing base fuel of hexane was employed. The boiling points for hexane, fluorobenzene, and DEMA are 338, 342 and 358 K, respectively, and the solution was composed of 89% hexane, 2% fluorobenzene and 9% DEMA by volume. The calculation and experimental conditions are shown in Table 1. The injection pressure of the injector was set to 5.1 MPa as rail pressure. The wall temperature was considered same to the ambient temperature. The injection duration and quantity were 2 ms and 15 mg, respectively. Fig. 4 shows the geometry of impingement wall. The impinging distance is 46.7 mm. The cavity diameter is 30 mm and the cavity angles are 0°, 30°, 60° and 90°. The computation domain is the 80 mm × 80 mm.

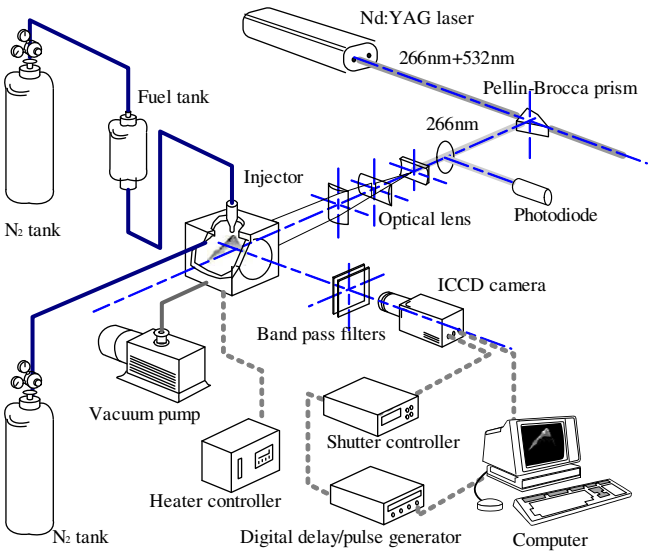


**Fig. 3.** Schematic of experimental setup.

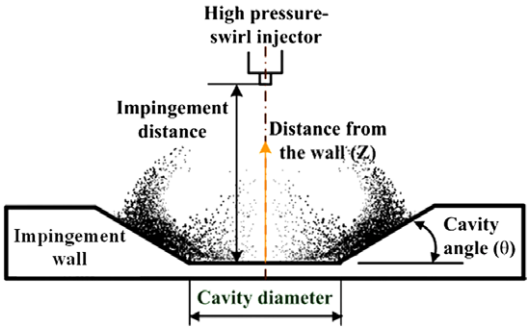


**Fig. 4.** Geometry of the impingement wall.

## 4. Validation of spray models

The validation of spray breakup, vaporization and wall impingement models was performed at various ambient conditions.

The validation of LISA–APTAB model was performed according to the spray tip penetration as shown in Fig. 5. The experimental spray tip penetration was determined as measuring the visible leading edge of the spray images. The calculated spray tip penetration was defined as the average distance of the leading 10 particles from the injector nozzle. Good agreements were found between the calculated and the experimental results, even though some discrepancies were observed.

It have been noticed that the vaporization model used in KIVA code shows discrepancies because of the late vaporization in early period after the start of injection. The phenomenon affects the liquid spray structure and tip penetration seriously. Hence, to validate the Abramzon model, a comparison between the calculated and experimental spray tip penetrations was performed as shown in Fig. 6. The calculated results showed similar tendency with experimental results. Therefore, the Abramzon model can be used in the calculation of spray vaporization.

Fig. 7 shows the validation of wall impingement mode by comparison of calculated and experimental radial distances at the ambient conditions of 0.1 and 0.5 MPa because wall impingement models affect the spray distribution after the spray–wall impingement. The experimental radial distance was determined as measuring the visible leading edge from injector center of the spray images. The calculated radial distance was defined as the average

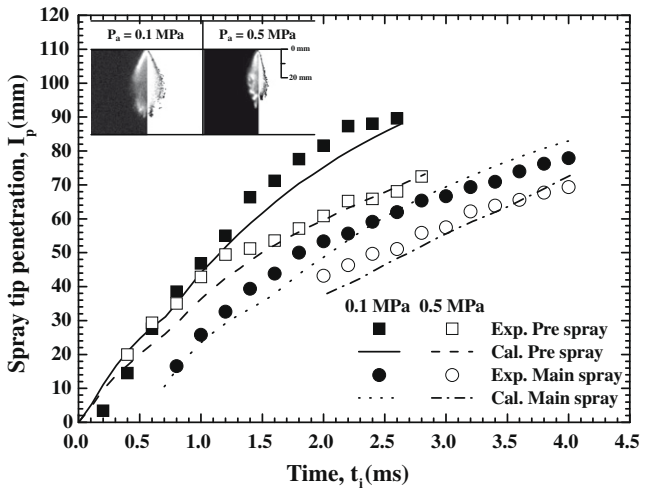


**Fig. 5.** The calculated and experimental spray tip penetrations at the ambient temperature of 293 K.

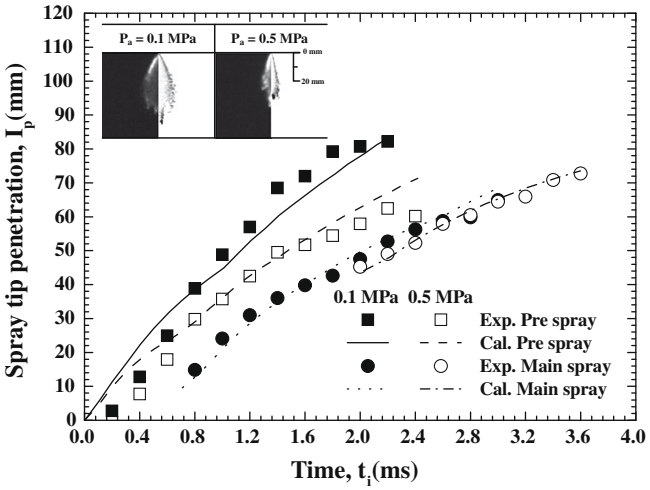


**Fig. 6.** The calculated and experimental spray tip penetrations at the ambient temperature of 473 K.

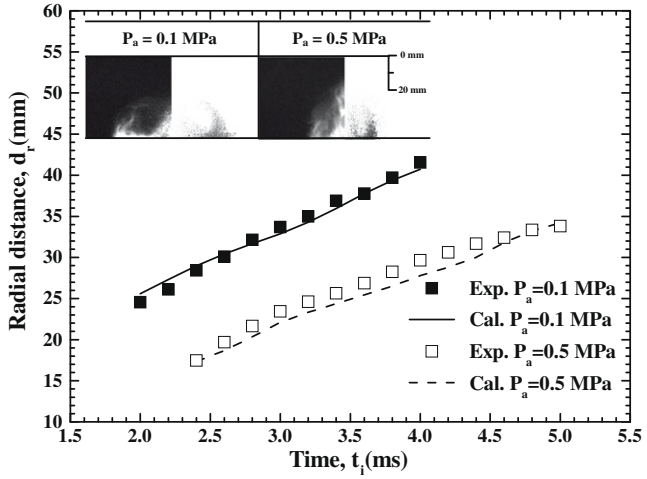


**Fig. 7.** The calculated and experimental radial distance after spray–wall impingement at the ambient temperature of 293 K.

distance of the leading 10 particles from the injector center. The calculated results were good agreement with the experimental results. From above results, the LISA–APTAB model, the Abramzon model and the Bai models can be used in the calculation of hollow-cone fuel spray.

## 5. Results and discussions

### 5.1. Non-vaporization conditions

The spray–wall impingement process at the ambient pressures of 0.1 and 0.5 MPa and the ambient temperature of 293 K was investigated.

Fig. 8 shows the calculated and experimental results of spray–wall impingement structure for 4.0 ms after the start of the injection. The left side images show the experimental results and the rights show the calculated results. The calculated results in the outer region of spray showed the similar tendency with experimental results. In the inner region of spray, however, the discrepancy between calculated and experimental results was observed. The calculated results showed the hollow-cone fuel spray but some droplets in experiment were distributed at the inner region of

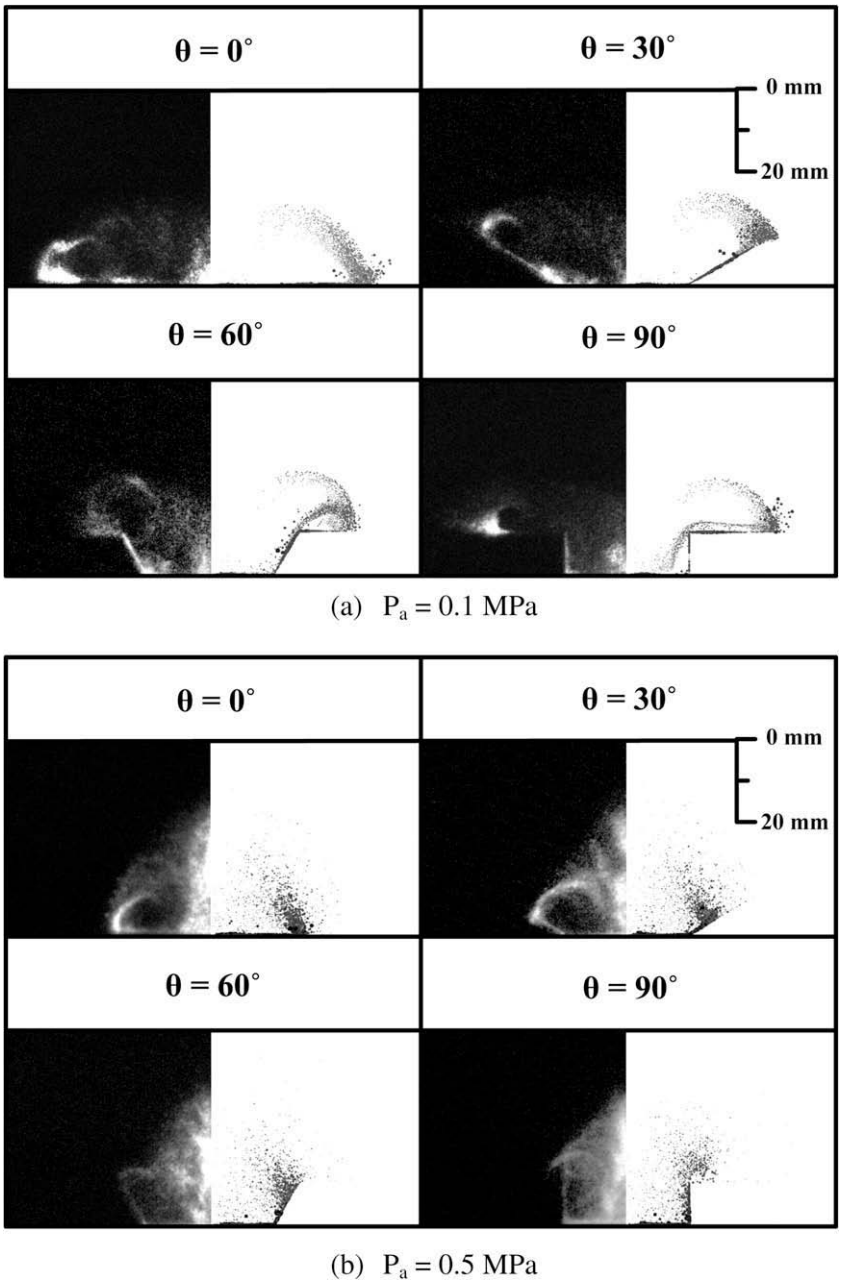


**Fig. 8.** The calculated and experimental results of impinging spray structure according to the wall geometry at the ambient pressures of 0.1 and 0.5 MPa and the ambient temperature of 293 K (left, experiments; right, calculations).

spray. Various cavity angles were applied to investigate the effect of the cavity angle on the spray–wall impingement process. The vortex cloud, which is caused by the gas flow circulating through the spray, was observed at the outer region of spray like as the case of free spray. The entraining gas flows as shown in Fig. 9 interact with the spray droplets and suppress the spray development and the gaseous vortex flow also tends to carry smaller droplets. Hence, the number density of droplets was higher at the vortex region. The vortex cloud was distributed near the cavity region in the case of the high cavity angle because the gaseous flow into the radial direction was weakened due to a momentum loss by the cavity wall. Also, the impinging radial distance became smaller with the increase of cavity angle because of the momentum loss by the cavity wall, while the difference of impinging spray height according the change of cavity angles was small. At the ambient pressure of 0.5 MPa, the most spray was distributed inside cavity region and could not grow toward the radial direction due to the high ambient density. It is expected that the higher spray concentration in the cavity region at the high ambient pressure have a great effect on the formation of fuel film at the wall surface and engine emissions.

Fig. 10 shows the radial distance after the wall impingement. The calculated results showed a similar tendency with the experimental results. Generally, the radial distance decreased with the increase of cavity angle because the resistance to the spray growth becomes larger with the increase of cavity angle. At the ambient pressure 0.1 MPa. however, the radial distance at the cavity angle of 90° was larger than the results at the cavity angles of 30° and 60° because the spray at the cavity angle of 90° was divided into inner and outer part of cavity after imping-

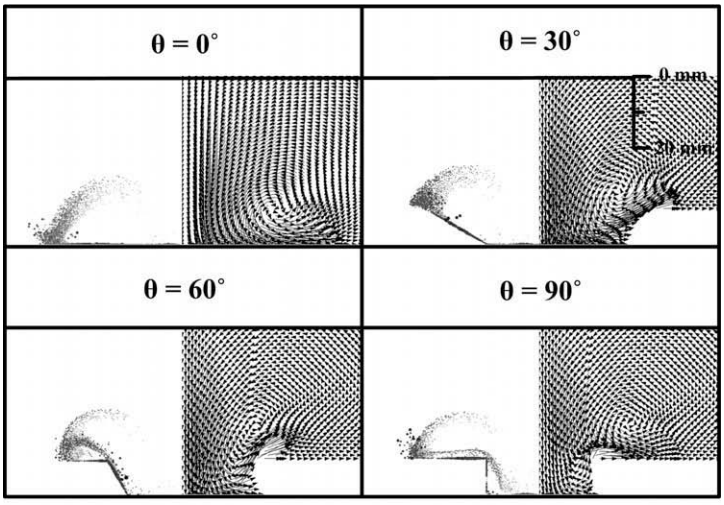


(a) $P_a = 0.1$ MPa

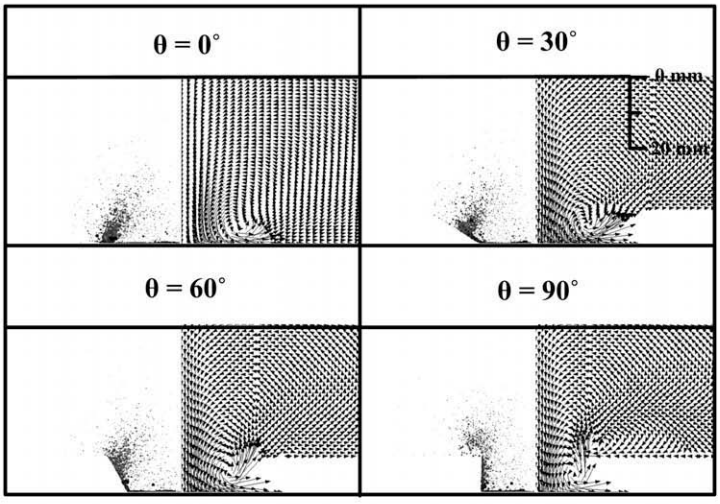


(b) $P_a = 0.5$ MPa

**Fig. 9.** The calculated results of the ambient gas velocity field at the ambient pressures of 0.1 and 0.5 MPa and the ambient temperature of 293 K (left, droplets; right, ambient gas velocity fields).

ing to the wall, and then the spray impinged at the outer region of cavity grew toward the radial distance without the resistance by the cavity wall. At the ambient pressure of 0.5 MPa, the radial distance decreased with the increase of cavity angle and most spray impinged at the inner area of the cavity due to narrower spray angle at the high ambient gas density. Also, the spray at the cavity angle of 90° did not divide into two parts and the radial distance was the narrowest at high ambient condition and the spray couldn't grow toward the radial direction from 3.0 ms after the injection. The difference of radial distance due to the cavity angle at the ambient pressure of 0.5 MPa was larger than it was at 0.1 MPa because the resistance by the cavity angle and high ambient gas density hiders the spray growth toward the radial direction at one time. Table 2 shows the decrease rate of radial distance according to the ambient pressure for 4.0 ms after the injection. On the whole, the decrease rates were larger at the cavity angles of 0° and 90° than those at 30° and 60°. This is because the spray growth at the ambient pressure of 0.1 MPa is affected by the only cavity wall but the ambient gas with low density does not affect the spray growth, while the high ambient gas density as well as the cavity angle affects the spray growth at the ambient pressure of 0.5 MPa.

Fig. 11 shows the calculated results of fuel film mass accumulated in the wall surface. The fuel film mass increased first from 1.0 ms after the injection and second increase was occurred from 2.0 ms. The first increase of fuel film mass resulted in the wall impingement of pre spray and the second increase was due to the impingement of main spray. At the ambient pressure of 0.1 MPa, according to the increase of cavity angle the fuel film mass also increased because the start time of impingement between main spray and wall became faster due to the decrease of distance from the injector tip to the cavity wall. At the ambient pressure of 0.5 MPa, the fuel film mass also increased with the cavity angle and more fuel film was observed than it was at the ambient pressure of 0.1 MPa because the spray is densely distributed near the wall due to the high density ambient gas and the cavity wall. On the other hand, the first impingement time of pre spray increased to 1.5 ms at the ambient pressure of 0.5 MPa because of the shorter penetration by the higher ambient gas density. Table 3 show the increase rate of fuel film mass according to the ambient pressure for 5.0 ms after the injection. Generally, the increase ratio became higher with the increase of cavity angle because the spray is densely distributed at high cavity angles. At the cavity angle of 30°, however, the increase rate was the lowest. This phenomenon is be-

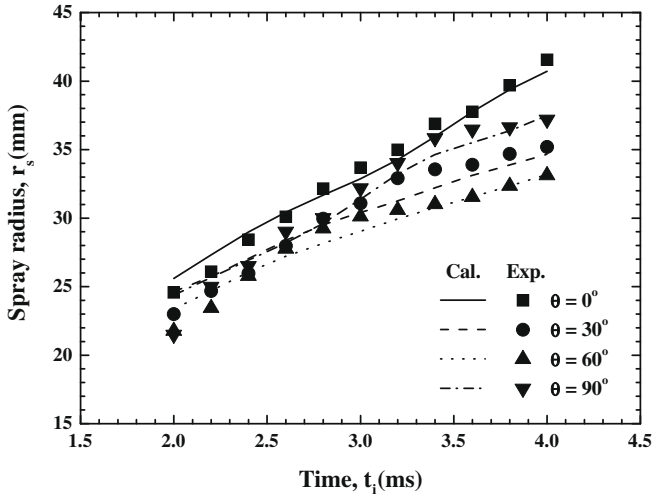


(a) $P_a$ = 0.1 MPa

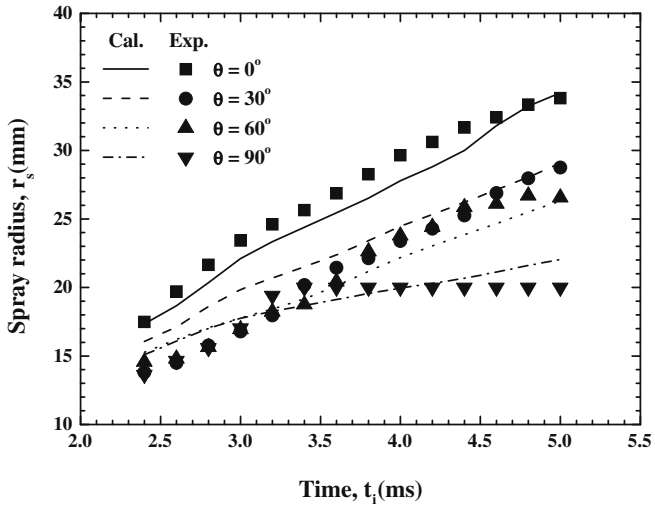


(b) $P_a$ = 0.5 MPa

**Fig. 10.** The calculated and experimental radial distance after spray–wall impingement at the ambient pressures of 0.1 and 0.5 MPa and the ambient temperature of 293 K.

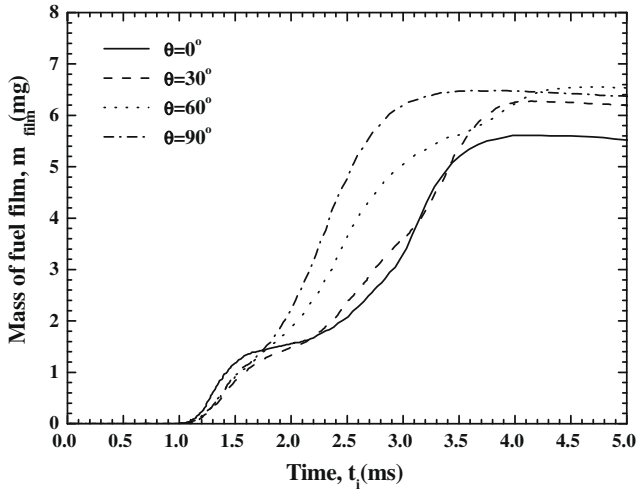


(a) $P_a$ = 0.1 MPa

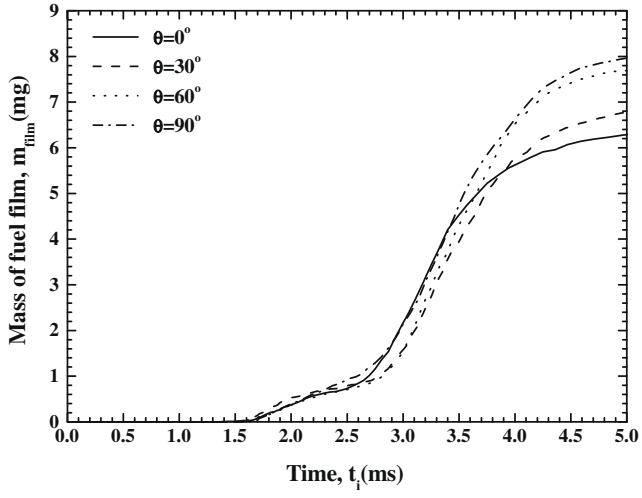


(b) $P_a$ = 0.5 MPa

**Fig. 11.** The calculated results of fuel film mass by spray–wall impingement at the ambient pressures of 0.1 and 0.5 MPa and the ambient temperature of 293 K.

**Table 2**
The decrease rate (%) of spray radius according to the ambient gas pressure for 4.0 ms after the injection.

| | 0° | 30° | 60° | 90° |
|---|---|---|---|---|
| Spray radius (mm) at 0.1 MPa | 40.7 | 34.7 | 33.2 | 37.5 |
| Spray radius (mm) at 0.5 MPa | 34.9 | 33.7 | 31.7 | 34.1 |
| Decrease rate (%) | 14.4 | 2.9 | 4.5 | 9.1 |

**Table 3**
The increase rate (%) of fuel film mass according to the ambient gas pressure for 5.0 ms after the injection.

| | 0° | 30° | 60° | 90° |
|---|---|---|---|---|
| Fuel film mass (mm) at 0.1 MPa | 5.52 | 6.19 | 6.54 | 6.37 |
| Fuel film mass (mm) at 0.5 MPa | 6.28 | 6.78 | 7.69 | 7.97 |
| Increase rate (%) | 13.7 | 9.5 | 17.6 | 25.1 |

**Table 4**
The calculated results of average SMD (μm) at the ambient temperature of 293 K.

| | | 0° | 30° | 60° | 90° |
|---|---|---|---|---|---|
| 3.0 ms | 0.1 MPa | 21.1 | 19.1 | 17.6 | 16.5 |
| | 0.5 MPa | 34.4 | 33.9 | 34.5 | 33.3 |
| 4.0 ms | 0.1 MPa | 19.8 | 17.2 | 18.8 | 17.1 |
| | 0.5 MPa | 32.6 | 31.4 | 31.4 | 30.0 |

cause the change of radial distance by the ambient pressure is the smallest at this condition as shown in Table 2.

Table 4 shows the calculated results of average Sauter mean diameter (SMD) of all droplets in a calculation domain for 3.0 and 4.0 ms after the start of the injection. At the ambient pressure of 0.5 MPa, the SMD was larger than it was at the ambient pressure of 0.1 MPa because the spray is densely distributed near the wall and the collision and coalescence phenomenon caused the increase of droplet size. On the whole, the SMD decreased according to the increase of the cavity angle, since the breakup process by the wall impingement of spray was more active at the high cavity angle. With elapse of time, the SMD became smaller because the droplets breakup by the interaction between spray and ambient gas and the

spray–wall impingement. However, in the case of the ambient pressure of 0.1 MPa and the cavity angle of 60° and 90°, the SMD became larger with elapse of time because the smaller droplets, which are distributed densely in the cavity region, collide and coalesce again each other and become larger.

### 5.2. Vaporization conditions

The vaporization process of impinging hollow-cone fuel spray at ambient pressures of 0.1 and 0.5 MPa and the ambient temperature of 473 K was analyzed by the experiment and calculation.

Fig. 12 shows the experimental and calculated results of spray–wall impingement structure at two ambient pressures and the vaporization condition for 4.0 ms after the start of the injection. Some discrepancies between the calculated and experimental results were observed, especially at the center region of spray, but the calculated results showed similar tendency with experimental results. All results by calculation and experiment did not show clearly. At the vaporization condition, the droplets were vaporized and its sizes decreased. As results, the number density of droplets became lower according to the increase of ambient temperature. The radial distance and spray height at the ambient temperature of 473 K became larger and lower than those at the ambient temperature of 293 K because the gas density at the ambient temperature of 473 K was lower and the spray growth was more active. The vortex cloud was observed at the more outer region of spray than it was at the lower ambient temperature due to small restriction of ambient gas density. At the ambient pressure of 0.5 MPa, the most droplets were distributed near the wall and adhered to the wall. This tendency affects the fuel film formation and emissions in GDI engines.

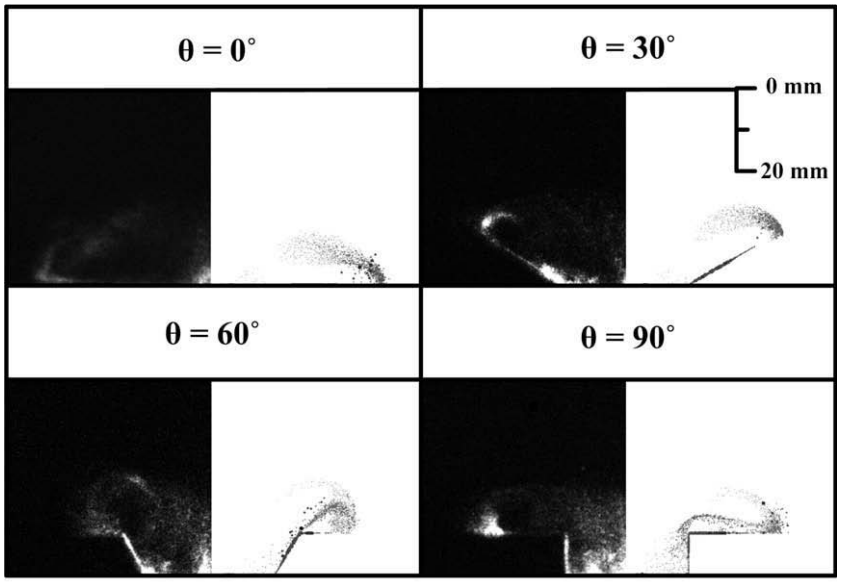


(a) $P_a = 0.1$ MPa

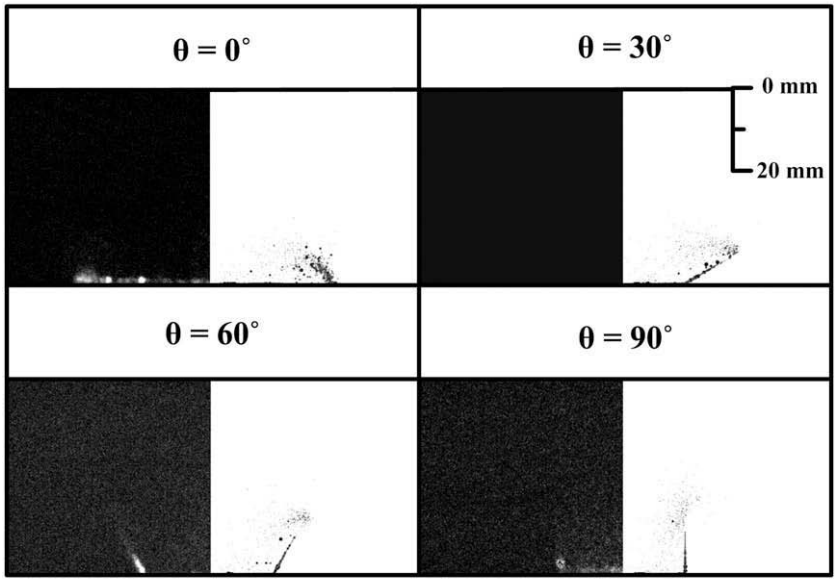


(b) $P_a = 0.5$ MPa

**Fig. 12.** The calculated and experimental results of impinging spray structure according to the wall geometry at the ambient pressures of 0.1 and 0.5 MPa and the ambient temperature of 473 K (left, experiments; right, calculations).

Fig. 13 shows the vapor phase distribution and the droplet distribution for 4.0 ms after the start of the injection. The vapor phase distribution was similar with the droplet distribution. There are many small droplets in the vortex region. These droplets vaporize easily and the vapor phase in this region was richer than that in other region. The vapor phase near the wall was also rich due to the effect of high wall temperature. On the other hand, the vapor phase in the center of spray was diluted because the droplet size in this region was larger due to the pre spray with large size and these droplets could not vaporize rapidly and the number density is also lower. According to the increase of the cavity angle, the vapor phase concentration became lower because the vaporization rate is lower at larger cavity angle due to dense distribution of droplets. The vapor phase at the high cavity angle was more distributed in the cavity region due to the restriction of cavity wall. The vapor phases at the high ambient pressure was observed lower than they were at the lower ambient pressure and most vapor phase was distributed in the cavity region because the vaporization times of larger droplets at the high ambient pressure become longer and the spray angle at the high ambient pressure is narrow. The high concentration of vapor phase was observed at the side wall of cavity with high temperature.

Fig. 14 shows the calculated results of fuel film mass by the spray–wall impingement. The fuel film mass increased after the spray–wall impingement and then decreased due to the vaporization at the high temperature conditions of ambient gas and wall. At the ambient pressure of 0.1 MPa, the first time of fuel film generation was about 1.2 ms after the injection and the generated fuel film was disappeared from 2.5 to 3.5 ms after the injection. As shown in Table 5, the life times were the shortest at the cavity an-

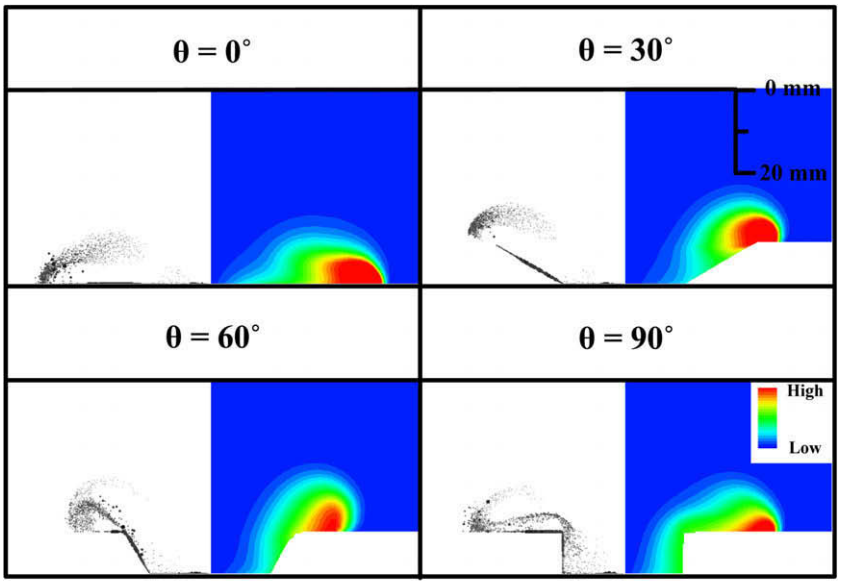


(a) $P_a = 0.1$ MPa

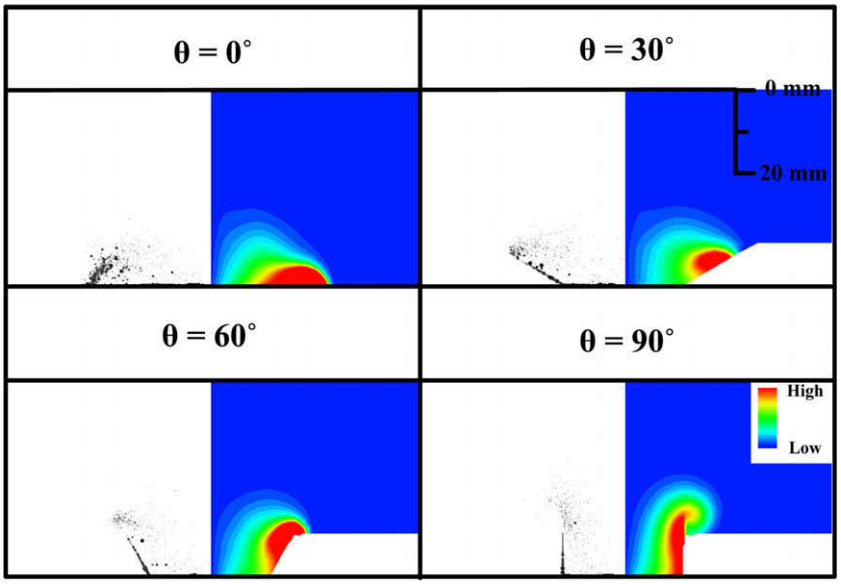


(b) $P_a = 0.5$ MPa

**Fig. 13.** The calculated results of vapor phase distribution at the ambient pressures of 0.1 and 0.5 MPa and the ambient temperature of 473 K (left, liquid phase; right, vapor phase).

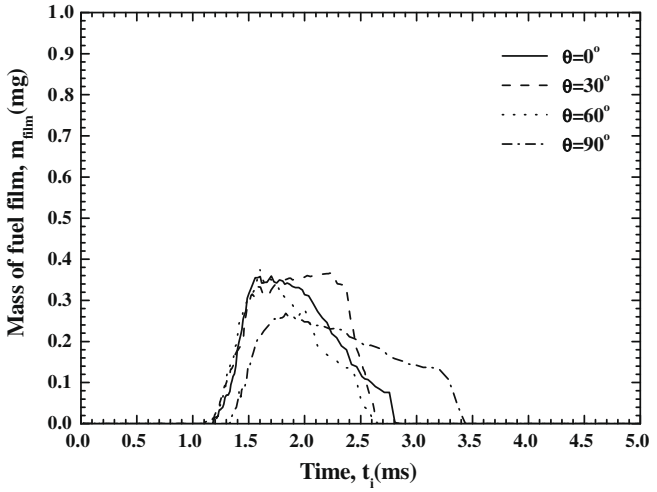


(a) $P_a$ = 0.1 MPa

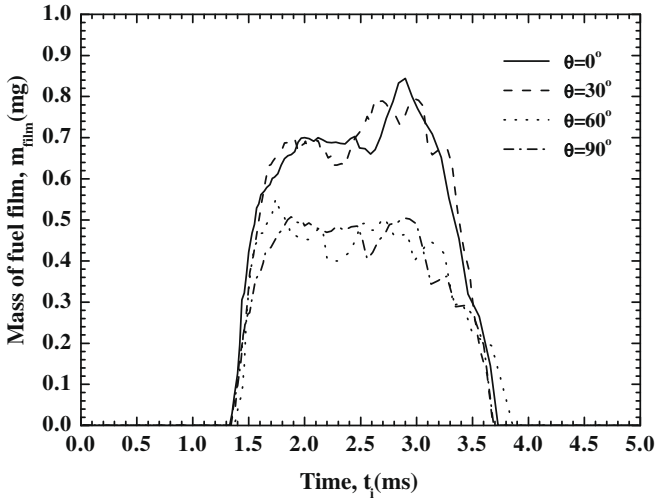


(b) $P_a$ = 0.5 MPa

**Fig. 14.** The calculated results of fuel film mass by spray–wall impingement at the ambient pressures of 0.1 and 0.5 MPa and the ambient temperature of 473 K.

**Table 5**
The life time (ms) of fuel film mass.

| | 0° | 30° | 60° | 90° |
|---|---|---|---|---|
| 0.1 MPa | 1.63 | 1.49 | 1.47 | 2.19 |
| 0.5 MPa | 2.31 | 2.32 | 2.37 | 2.24 |

gles of 30° and 60° and life time at the cavity angle of 90° was the longest. This is because the impinging droplets at the cavity angle of 90° could not grow toward the radial direction and these droplets were densely adhered to the wall in the cavity and formed thick fuel film. At the ambient pressure of 0.5 MPa, the droplet size was larger than that at the low ambient pressure condition and the heating and vaporization times of these large droplets was longer and the fuel film is distributed densely and thickly. Accordingly, more fuel film mass was observed than that at the low ambient pressure. The fuel film distribution was similar at all cavity angles, therefore, the cavity angle did not affect to the life time of fuel film as shown in Table 5.

Table 6 shows the calculated results of average SMD for 3.0 and 4.0 ms after the start of the injection. The SMD decreased with the increase of ambient gas temperature by the spray vaporization. The SMD is larger at the high ambient pressure due to dense distribution of droplets and decreased with the increase of cavity angle. At the ambient pressure of 0.1 MPa, the SMD at the cavity angles of 0° and 30° became smaller with time, while the SMD at the cavity angles of 60° and 90° became larger with time due to the collision and coalescence among droplets, that is, the droplets at these conditions were densely distributed.

**Table 6**
The calculated results of average SMD (μm) at the ambient temperature of 473 K.

| | | 0° | 30° | 60° | 90° |
|---|---|---|---|---|---|
| 3.0 ms | 0.1 MPa | 19.0 | 17.7 | 16.1 | 15.4 |
| | 0.5 MPa | 28.9 | 28.8 | 27.6 | 26.2 |
| 4.0 ms | 0.1 MPa | 15.9 | 13.9 | 16.2 | 16.1 |
| | 0.5 MPa | 27.7 | 25.0 | 20.8 | 18.4 |

## 6. Conclusions

The atomization, vaporization and wall impingement processes of the hollow-cone fuel spray at various ambient conditions and wall geometries were analyzed with the numerical and experimental methods. Following summarizes the results:

(1) The vortex due to the interaction with the ambient gas was observed and it grew toward the radial direction. According to the increase of cavity angle, the spray was densely distributed in the cavity region. Most spray was distributed in the cavity region at the ambient pressure of 0.5 MPa. In the case of the ambient temperature of 473 K, the spray was distributed near the wall and the growth was more active than it was at the lower ambient temperature.
(2) The radial distance after the wall impingement was smaller at the high cavity angle and the high ambient temperature. However, at the ambient pressure 0.1 MPa, the radial distance at the cavity angle of 90° was longer than it was at the cavity angles of 30° and 60°. The spray growth toward the radial direction was weakened at the high ambient pressure.
(3) The SMD was smaller at the high ambient temperature by the spray vaporization and increased at the high ambient pressure. On the whole, the SMD decreased with the increase of cavity angle.
(4) The fuel film was formed at the wall and its mass became higher at the high cavity angle and the high pressure. The generated fuel film was vaporized rapidly at the high ambient temperature.
(5) The vapor phase was distributed similar to the droplets distribution. The high concentration region of vapor phase distribution was observed at the region with numerous droplets.

## Acknowledgement

This work was supported by the research project [2007-C-CD12-P-01-3-010] of the Korea Energy Management Corporation.

## References

Abramzon, B., Sirignano, W.A., 1989. Droplet vaporization model for spray combustion calculation. Int. J. Heat Mass Transfer 32, 1605–1618.
Amsden, A., 1997. KIVA-3V: A Block-Structured KIVA Program for Engines with Vertical or Canted Valves, Los Alamos National Laboratory Report LA-13313-MS.

Bai, C., Gosman, D., 1995. Development of methodology for spray impingement simulation. SAE Paper 1995, 950283.
Dombrowski, N., Hooper, P.C., 1962. The effect of ambient density on drop formation in sprays. Chem. Eng. Sci. 17, 291–305.
Drake, M.C., Fansler, T.D., Solomon, A.S., Szekely, G.A.J., 2003. Piston fuel films as a source of smoke and hydrocarbon emissions from a wall-controlled spark-ignited direct-injection engine. SAE Paper, 2003-01-0547.
Han, Z., Reitz, R.D., 1995. Turbulence modeling of internal combustion engines using RNG k–e models. Combust. Sci. Technol. 106, 267–295.
Lindgren, R., Denbratt, I., 2000. Modelling gasoline spray–wall interaction – a review of current models. SAE Paper, 2000-01-2808.
Liu, A.B., Mather, D., Reitz, R.D., 1993. Modeling the effects of drop drag and breakup on fuel sprays. SAE Paper, 930072.
O'Rourke, P.J., 1981. Collective Drop Effects on Vaporizing Liquid Sprays. Ph.D. Dissertation, Princeton University.
Park, J.S., Xie, X., Im, K.S., Kim, H.S., Las, M.C., Yang, J.L., Han, Z.Y., Anderson, R.W., 1999. Characteristics of direct-injection gasoline spray wall impingement at elevated temperature conditions. SAE Paper, 1999-01-3662.
Senda, J., Kobayashi, M., Iwashita, S., Fujiomoto, H., 1994. Modeling of diesel spray impingement on a flat wall. SAE Paper, 941894.
Shim, Y.S., Choi, G.M., Kim, D.J., 2008. Development and validation of a new hybrid break-up model for the modelling of hollow-cone fuel spray. Proc. Inst. Mech. Eng. D J. Autom. Eng. 222, 275–284.
Walkins, A.P., Park, K., 1996. Assessment and application of a new spray wall impaction model. Proc. Inst. Mech. Eng. Conf. Comput. Reciprocating Gas Turbines, 1–10.
Zhao, F., Lai, M.C., Harrington, D.L., 1999. Automotive-spark ignited direct-injection gasoline engines. Prog. Energy Combust. Sci. 25, 427–532.